Distribution Agreement

In presenting this thesis as a partial fulfillment of the requirements for a degree from Emory University, I hereby grant to Emory University and its agents the non-exclusive license to archive, make accessible, and display my thesis in whole or in part in all forms of media, now or hereafter now, including display on the World Wide Web. I understand that I may select some access restrictions as part of the online submission of this thesis. I retain all ownership rights to the copyright of the thesis. I also retain the right to use in future works (such as articles or books) all or part of this thesis.

Cameron I Cohen April 9, 2021

Bisphosphonate-conjugated silica nanoparticle internalization and localization patterns in osteoclast and osteoblast precursor cells

by

Cameron I Cohen

George Beck
Adviser

Department of Biology

George Beck

Adviser

M Neale Weitzmann

Committee Member

Eladio Abreu

Committee Member

Jamie Arnst

Committee Member

2021

Bisphosphonate-conjugated silica nanoparticle internalization and localization patterns in osteoclast and osteoblast precursor cells

By

Cameron I Cohen

George Beck

Adviser

An abstract of
a thesis submitted to the Faculty of Emory College of Arts and Sciences
of Emory University in partial fulfillment
of the requirements of the degree of
Bachelor of Science with Honors

Department of Biology

2021

Abstract

Bisphosphonate-conjugated silica nanoparticle internalization and localization patterns in osteoclast and osteoblast precursor cells

By Cameron I Cohen

In the past decade, Nanotechnology has emerged as an important novel strategy for drug delivery and therapeutic intervention. Silica nanoparticles especially have proven revolutionary in the realm of bone biology. Their ability to be readily internalized in bone cells and general biocompatibility open up opportunities for new bone disease treatments, such as osteoporosis. Bioactive, OH-terminated silica nanoparticles are particularly promising due to their ability to affect the differentiation of osteoblasts and osteoclasts *in vitro*. As opposed to current osteoporosis drugs which only suppress osteoclast activity, these nanoparticles are unique in their ability to inhibit osteoclast differentiation, the cells responsible for bone resorption, and stimulate osteoblast differentiation, the cells responsible for bone formation. Additionally, the nanoparticles have been shown to increase bone density in mice *in vivo*. However, to improve targeting to the bone, and thereby increase efficacy, a modified nanoparticle with alendronate, a bisphosphonate used for osteoporosis, on the surface was designed. In this study, we show that OH-terminated silica nanoparticles and bisphosphonate-conjugated nanoparticles exhibit similar internalization patterns with respect to time and concentration in both pre-osteoclast RAW 264.7 and pre-osteoblast MC3T3-E1 cell lines. Endocytosis studies also indicate shared internalization pathways between the two particles and colocalization assays identify shared localization patterns. In addition, XTT assays demonstrate no decrease in viability for cells treated with bisphosphonate-conjugated silica nanoparticles. These studies pave the way for future functional assays and provides the first step in elucidating the characteristics and mechanistic behavior of the newly developed bisphosphonate-conjugated nanoparticle. As opposed to merely slowing the degradation of bone, our nanoparticle would have the ability to restore lost bone density. Combined with improved targeting to the bone, this nanoparticle has the potential to be a highly effective new treatment for osteoporosis.

Bisphosphonate-conjugated silica nanoparticle internalization and localization patterns in osteoclast and osteoblast precursor cells

By

Cameron I Cohen

George Beck

Adviser

A thesis submitted to the Faculty of Emory College of Arts and Sciences
of Emory University in partial fulfillment
of the requirements of the degree of
Bachelor of Science with Honors

Department of Biology

2021

Acknowledgements

This study was supported by a grant from the NIH (R21AR073593). The author would like to thank Hong Yi of the Robert P. Apkarian Integrated Electron Microscopy Core at Emory University for expert technical assistance associated with TEM.

The author would also like to thank Jamie Arnst in particular for her constant help and support throughout the thesis process, as well as all of the other committee members for their input and guidance.

Table of Contents

Introduction 1

Materials and methods 2

- Silica nanoparticle synthesis 2
- Characterization of silica nanoparticles 2
- Cell culture and reagents 2
- Dose-response internalization assays 2
- Time-course internalization assays 3
- Endocytosis assays 3
- Colocalization assays 4
- XTT assays 4
- Fluorescence microscopy imaging 4
- Statistical analysis 4

Results 4

- Silica nanoparticle characterization 4
- Dose-dependent internalization of OH-terminated and bisphosphonate-conjugated silica nanoparticles 5
- Time-dependent internalization of OH-terminated and bisphosphonate-conjugated silica nanoparticles 5
- Endocytosis assay of bisphosphonate-conjugated silica nanoparticles 6
- Colocalization assay of bisphosphonate-conjugated silica nanoparticles 7
- XTT assay of bisphosphonate-conjugated silica nanoparticles 7

Discussion 17

Conclusion 19

References 20

List of Figures

Figure

1: Characterization of OH-terminated silica nanoparticles and bisphosphonate-conjugated silica nanoparticles 8

2: Dose-response internalization of OH-terminated and bisphosphonate-conjugated silica nanoparticles in RAW 264.7 cells 9

3: Dose-response internalization of OH-terminated and bisphosphonate-conjugated silica nanoparticles in MC3T3-E1 cells..... 10

4: Time-course internalization of OH-terminated and bisphosphonate-conjugated silica nanoparticles in RAW 264.7 cells 11

5: Time-course internalization of OH-terminated and bisphosphonate-conjugated silica nanoparticles in MC3T3-E1 cells..... 12

6: Dose-response and time-course assays in RAW 264.7 and MC3T3-E1 cells 13

7: Endocytosis assays of bisphosphonate-conjugated silica nanoparticles in RAW 264.7 cells..... 14

8: Localization assays of bisphosphonate-conjugated silica nanoparticles in RAW 264.7 cells..... 15

9: XTT viability assays of bisphosphonate-conjugated silica nanoparticles in RAW 264.7 cells..... 16

1. Introduction

Nanoparticles have been used in the scientific community for a vast array of purposes but are of special interest in the realm of biology and medicine. Already, nanoparticles have shown potential in therapeutic applications, such as selective drug delivery [1, 2]. Silica nanoparticles in particular are able to accommodate many physical modifications including differing size, charge, and incorporation of compounds which makes them an exciting candidate for therapeutic development [3, 5, 15]. Currently, the most common applications for silica nanoparticles in particular lie in drug-delivery and bone-repair due in part to its biocompatibility with the unique structure of the bone microenvironment [4, 16, 22].

Bone health and integrity play a large role in not only maintaining the structural frame of the body and protecting organs but many biological functions such as fostering immune and blood cells [6]. Therefore, maintaining bone health is vital for overall fitness. Osteoporosis, and bone disease, are characterized by a loss of bone density that often results in multiple fractures [7, 8]. Studies have additionally shown increased mortality rates associated with osteoporotic patients even after low-trauma fracture [26]. The loss of bone density is due to an imbalance in osteoclast and osteoblast activity which results in lowered bone-forming osteoblast activity, and increased bone-resorbing osteoclast activity [7, 8]. Current osteoporosis treatments often only target osteoclasts by inhibiting their activity which can slow the degradation of bone but fails to restore lost bone density [9].

Silica nanoparticles have been shown to act on the differentiation of both types of bone cells [10]. Previous studies have demonstrated the ability of silica nanoparticles to interfere in the autophagy pathways of bone cells which lead to an increase in osteoblast differentiation and a decrease in osteoclast differentiation in cell cultures [10, 11]. Silica nanoparticles were even shown to restore bone density in young and old osteoporotic mice models when given intraperitonially [12]. However, previous studies have demonstrated that silica nanoparticles administered orally tend to experience widespread absorption in the body, especially in the spleen, kidneys, liver, and lungs [23, 27].

In order to improve orally administered drug targeting to the bone, a new silica nanoparticle was developed with a bisphosphonate, alendronate, bound to the surface [28]. Alendronate is a commercially available osteoporosis drug that is ingested orally and has been shown to prevent bone loss through suppression of osteoclast activity [13]. This study aims to investigate the characteristics of a newly developed bisphosphonate-conjugated silica nanoparticle which will ideally improve targeting to the bone [28]. Here we first use a series of internalization assays to compare the ability of bone cells to take up OH-terminated silica nanoparticles and bisphosphonate-conjugated silica nanoparticles in a dose and time-dependent manner. Even further, endocytosis assays will assess the method by which osteoclasts take up the two nanoparticles. Endocytosis typically occurs using any of three primary pathways including lipid raft/caveolae, clathrin-mediated, and macropino/phagocytosis [17]. In a previous study, OH-terminated silica nanoparticles have been shown to predominantly utilize the caveolae/lipid raft-mediated pathway for internalization in MC3T3-E1 cells [11]. The same inhibitors will be used to assess and compare bisphosphonate-conjugated nanoparticle's primary method of internalization RAW 264.7 cells. Similarly, the same markers used in previous studies on OH-terminated silica nanoparticles in MC3T3-E1 cells will be used to assess the localization of bisphosphonate-conjugated nanoparticles in RAW 264.7 cells [11].

As the conjugation of alendronate to the silica nanoparticle surface alters the surface characteristics, it is vital to determine if the functional capabilities of the newer bisphosphonate-conjugated nanoparticle matches that of the previous OH-terminated silica nanoparticle. Previous studies have shown that an alteration of surface characteristics can alter nanoparticle-cell interactions, especially in RAW 264.7 cells [15]. While internalization characteristic assays provide some valuable information, further functional assays such as tartrate-resistant acid phosphatase (TRAP) staining, alkaline phosphatase (ALP) staining, and PCR for genes involved in differentiation and autophagy are required to determine if OH-terminated and bisphosphonate-conjugated silica nanoparticles have similar modes of action in bone *in vitro* and *in vivo*. In addition, viability assays such as XTT help determine the potential toxicity of the bisphosphonate-conjugated silica nanoparticle. This study provides an important first step in the characterization of bisphosphonate-conjugated silica nanoparticles in osteoclast and osteoblast precursor cells.

2. Materials and Methods

2.1 Silica nanoparticles synthesis

Bisphosphonate-conjugated 50nm silica nanoparticles (DNG-L228) and OH-terminated silica nanoparticles (DNG-L010) were synthesized for us by Creative Diagnostics and supplied in water (Alpharetta, GA). Alendronate was the bisphosphonate used in the synthesis of bisphosphonate-conjugated silica nanoparticles. Both nanoparticles were also synthesized with Rhodamine B dye inside the silica nanoparticle for use in fluorescence microscopy.

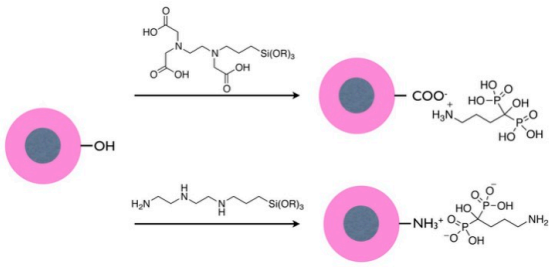

Methods of Alendronate conjugation to OH-terminated silica nanoparticle by electrostatic interaction [25]

2.2 Characterization of silica nanoparticles

The shape of both nanoparticles was characterized using transmission electron microscopy (TEM) (JEOL JEM-1400 Peabody, MA) performed by the Integrated Electron Microscopy Core at Emory University. Size measurements were obtained using dynamic light scattering (DLS) in water.

2.3 Cell culture and reagents

The murine macrophage/monocyte (pre-osteoclast) cell line RAW264.7 [14] and the murine pre-osteoblast cell line MC3T3-E1 [30] were obtained from ATCC (Manassas, VA). MC3T3-E1 cells were cultured in growth medium; α-Modified Eagle's Medium (α-MEM; Thermo Scientific; CN:12571048) supplemented with 50U/ml penicillin, 50 mg/ml streptomycin and 10% fetal bovine serum (FBS; Atlanta Biologicals, Lawrenceville, GA). RAW264.7 cells were culture in growth medium; Dulbecco's Modified Eagle's Medium (DMEM; Thermo Scientific; CN:11054001) supplemented with 50U/ml penicillin, 50 mg/ml streptomycin and 10% FBS. All cells were cultured at 37 °C in 5% CO_2.

2.4 Dose-response internalization assays

MC3T3-E1 cells were seeded at 20,000 cells/well in a 24-well plate. After 24 hours, cells were treated with either bisphosphonate-conjugated or OH-terminated silica nanoparticles at 100, 50, 25, 12.5, 6.25, 3.125, and 0 μg/ml concentrations. The next day cells were washed twice with PBS, fixed with formalin for 5 minutes, and stored in PBS. RAW264.7 cells were seeded at 50,000 cells/well in a 24-well plate. After 24 hours, cells were treated with either OH-terminated silica nanoparticles or bisphosphonate-conjugated nanoparticles at 100, 50, 25, 12.5, 6.25, and 3.125 μg/ml concentrations. The next day, cells were washed twice with PBS, fixed with formalin for 5 minutes, and stored in PBS. The time-course assay with RAW264.7 cells was repeated twice more under the same conditions. Analysis was done by quantifying the mean gray value of cells in each treatment group. Three different fields of view from each treatment well were imaged in brightfield and rhodamine red fluorescence. Using Fiji ImageJ, the mean gray value was measured for approximately 50 cells in each RAW 264.7 treatment group and approximately 30 cells in each MC3T3-E1 treatment group, keeping cell area consistent for each experiment. Once the background was subtracted from each individual mean gray value, the measurements for each treatment group were averaged between all three experiments.

2.5 Time-course internalization assays

MC3T3-E1 cells were seeded at 20,000 cells/well in a 24-well plate. After 24 hours, cells were treated with either 100μg/ml bisphosphonate-conjugated silica nanoparticles or 100μg/ml OH-terminated silica nanoparticles. At 24hr, 8hr, 4hr, 2hr, 1hr, 30min, and 15min time points, cells were washed twice with PBS, fixed with formalin for 5 minutes at 37˚C, and stored in PBS. RAW264.7 cells were seeded at 50,000 cells/well in a 24-well plate. After 24 hours, cells were treated with either 100μg/ml bisphosphonate-conjugated or OH-terminated silica nanoparticles. At 24hr, 8hr, 4hr, 2hr, 1hr, 30min, and 15min time points, cells were washed twice with PBS, fixed with formalin for 5 minutes, and stored in PBS. The dose-response assay with RAW264.7 cells was repeated twice more under the same conditions. Analysis was done by quantifying the mean gray value of cells in each treatment group. Three different fields of view from each treatment well were imaged in brightfield and rhodamine red fluorescence. Using Fiji ImageJ, the mean gray value was measured for approximately 50 cells in each RAW 264.7 treatment group and approximately 30 cells in each MC3T3-E1 treatment group, keeping cell area consistent for each experiment. Once the background was subtracted from each individual mean gray value, the measurements for each treatment group were averaged between all three experiments. All relative fluorescence values were then calculated as a percentage of total fluorescence.

2.6 Endocytosis assays

RAW 264.7 cells were seeded at 50,000 cells/well in a 24-well plate in triplicate. After 24 hours, cells were pretreated for 2 hours with either 1mM Amiloride, 10μM Cytochalasin D, 25μM Chlorpromazine, 0.5μM Phenylarsine, 50μM Nystatin, or 7.5mM Methyl ß-cyclodextrin (MßCD) [11, 17]. Cells were then treated with 25μg/ml NP-OH or NP-BisPO4 and incubated for a further two hours. Cells were washed twice in PBS before imaging. Rates of internalization were analyzed by comparing the average relative fluorescent intensity (RFU) of 75 cells taken from three separate images to that of the control using ImageJ software [31].

2.7 Colocalization assays

Endocytic trafficking was measured using recycling of FITC-conjugated transferrin from human serum (Invitrogen). RAW 264.7 cells were washed once with PBS and incubated with internalization media (HBSS, 10mM HEPES [7.5]) and 10µg/ml NP-$BisPO_4$ for 2 hours. Cells were then allowed to take up FITC-transferrin (25µg/ml) at 37°C for 30 minutes. For lysosomal internalization, cells were incubated with 10µg/ml NP overnight, then washed twice and incubated in internalization media for 4 hours to improve lysosomal staining. 100nM LysoTracker Green (Invitrogen) was then added to the cells and incubated for 30 minutes. Hoechst 33342 (Envigo) was used to counter stain nuclei. Images of at least three different fields of view were taken. Colocalization analysis was performed using Fiji ImageJ plugin Coloc and the Pearson correlation coefficient was determined for five cells per field of view.

2.8 XTT assays

RAW 264.7 cells were seeded at 5000 cells/well in 96-well plates. After 24 hours, cells were treated with either bisphosphonate-conjugated or OH-terminated silica nanoparticles at 100, 50, 25, 12.5, 6.25, 3.125, and 1.5 µg/ml concentrations or Alendronate at 100, 50, 25, 10, 5, 1, 0.5, and .1uM concentrations. After either 24 or 48 hours, CellTiter 96 AQueous One Soultion Reagent (Promega) was added following manufacture's instructions and quantitated by spectrophometer (VersaMax microplate reader; Molecular Devices, San Jose, CA). Percent viability was determined using the following formula: 100% X (treated cells/average control cells).

2.9 Fluorescence microscopy imaging

All dose-response, time-course, endocytosis and colocalization assays images were using a Nikon Eclipse Ti2 (DAPI, FITC, TRITC filter cube set). Three fields of view from each well were imaged at either 10x or 20x magnification for dose-response, time-course, and endocytosis and 60x magnification for colocalization assays.

2.10 Statistical analysis

Data is represented as mean ± standard deviation unless otherwise noted. Statistical analysis was performed using GraphPad Prism 8.0 (La Jolla, California). Comparisons of treated cells were against the negative control, unless otherwise noted, using Student's T-test. *<0.005, **<0.0001

3. Results

3.1 Silica nanoparticle characterization

To determine the effects of using bisphosphonates to help target our OH-terminated silica nanoparticle, we conjugated alendronate to the surface of the OH-terminated silica nanoparticle. These particles were characterized for their shape and size. Both OH-terminated and bisphosphonate-conjugated silica nanoparticles were imaged with transmission electron

microscopy (TEM), which revealed largely spherical nanoparticles. Based on the images, the size of OH-terminated nanoparticles are predicted to be 42.4±9.2 nm and the size of bisphosphonate-conjugated silica nanoparticles are 40.6±7.8 nm. The nanoparticles were sent to Georgia Tech to determine size and charge via dynamic light scattering (DLS) and zeta potential. We anticipate that the size determined by DLS will be consistent with the TEM and expect the bisphosphonate-conjugated nanoparticle to have a more negative charge than the OH-terminated nanoparticle.

3.2 Dose-dependent internalization of OH-terminated silica nanoparticles and bisphosphonate-conjugated silica nanoparticles

Dose-dependent studies were conducted to assess the differences in nanoparticle internalization at different concentrations. The range of concentrations was also used to determine the EC_{50} for both nanoparticles which allows us to understand the dose-dependent internalization of our newest nanoparticle and provide a basis to determine effective treatment concentrations. Cells were treated at 100, 50, 25, 12.5, 6.25, 3.125, or 0 μg/ml and the relative fluorescence of each treatment group were determined.

In RAW 264.7 cells, both the OH-terminated silica nanoparticles and bisphosphonate-conjugated silica nanoparticles had relative fluorescence values that increased positively in a dose-dependent manner. There was no statistically significant difference between the two nanoparticles at any concentration. Comparisons of the fluorescence between both nanoparticles are depicted visually in Figure 2 and graphically in Figure 6. EC_{50} analysis for the OH-terminated nanoparticles is 40.9 ± 4.6 μg/ml and the bisphosphonate-conjugated nanoparticles 33.4 ± 6.3 μg/ml which seems to imply that bisphosphonate-conjugated nanoparticles exhibit slightly faster internalization patterns in RAW 264.7 cells as compared to OH-terminated silica nanoparticles.

In MC3T3-E1 cells, both the OH-terminated silica nanoparticles and bisphosphonate-conjugated silica nanoparticles also had relative fluorescence values that increased positively with increasing concentration values. Compared to OH-terminated silica nanoparticles, the bisphosphonate-conjugated silica nanoparticles had statistically higher levels of fluorescence at all concentrations, although this becomes less significant at the highest concentrations. Comparisons of the fluorescence between both nanoparticles are depicted visually in Figure 3 and graphically in Figure 6. Additionally, EC_{50} analysis was determined to be 46.08 ±1 0.5 μg/ml and 207.7 ± 224.6 μg/ml for bisphosphonate-conjugated and OH-terminated silica nanoparticles, respectively. Unlike in RAW 264.7 cells, we do not observe fluorescent saturation at the higher concentrations of nanoparticle in MC3T3-E1 cells, particularly with the OH-terminated nanoparticle. This suggests that the bisphosphonate-conjugated silica nanoparticle has greater internalization in MC3T3-E1 cells compared to the OH-terminated. However, additional studies using higher concentrations of nanoparticles are needed to confirm.

Overall, both nanoparticles exhibit similar dose-dependent patterns of internalization in RAW 264.7 cells and bisphosphonate-conjugated silica nanoparticles exhibit slightly faster internalization in MC3T3-E1 cells. It is also interesting to note that both nanoparticles exhibited much lower levels of internalization in MC3T3-E1 cells as compared to RAW 264.7 cells.

3.3 Time-dependent internalization of OH-terminated silica nanoparticles and bisphosphonate-conjugated silica nanoparticles

Time-dependent studies were conducted to assess the differences in nanoparticle internalization at different time points. An understanding of the time-dependent internalization of our newest nanoparticle will then allow us to determine effective treatment time points for future studies. Cells were treated at 24hr, 8hr, 4hr, 2hr, 1hr, 30min, and 15min time points and the relative fluorescence of each treatment group were determined and then calculated as a percentage of total fluorescence.

In RAW 264.7 cells, both the OH-terminated silica nanoparticles and bisphosphonate-conjugated silica nanoparticles had relative fluorescence percentage values that increased positively with increasing time points. There was no statistically significant difference between the two nanoparticles at any concentration. Comparisons of the fluorescence percentage between both nanoparticles are depicted visually in Figure 4 and graphically in Figure 6.

In MC3T3-E1 cells, both the OH-terminated silica nanoparticles and bisphosphonate-conjugated silica nanoparticles also had relative fluorescence percentage values that increased positively with increasing concentration values. Bisphosphonate-conjugated nanoparticles had statistically higher levels of fluorescence at 1, 2, 4 and 8 hours, but the difference was not significant at earlier time points or 24 hours. Comparisons of the fluorescence between both nanoparticles are depicted visually in Figure 5 and graphically in Figure 6.

Overall, both nanoparticles exhibit similar dose-dependent patterns of internalization in RAW 264.7 cells and bisphosphonate-conjugated silica nanoparticles exhibit slightly faster internalization in MC3T3-E1 cells for certain time points. However, it is also interesting to note that both nanoparticles exhibited much lower levels of internalization in MC3T3-E1 cells as compared to RAW 264.7 cells.

3.4 Endocytosis assay of bisphosphonate-conjugated silica nanoparticles

Endocytosis assays were conducted to elucidate the method of nanoparticle internalization. While the previous studies have focused primarily on the pathway used to internalize OH-terminated silica nanoparticles in MC3T3-E1 cells, endocytosis studies with bisphosphonate conjugated silica nanoparticles in RAW 264.7 cells still provide a basis for comparison between the two nanoparticles [11]. While the cell lines themselves are different, they likely share processes of internalization [32].

Inhibitors from the three major endocytosis pathways were used at varying concentrations. To test for endocytosis with the lipid raft/caveolae pathway, cells were treated with 7.5mM MßCD and 50μM Nystatin. For the clathrin-mediated pathway, 0.5μM Phenylarsine oxide and 25μM Chlorpromazine were used. Finally, for the macropino/phagocytosis pathway, cells were treated with 1mM Amiloride and 10μM Cytochalasin D.

For all three pathways, addition of the inhibitor resulted in a decrease in fluorescence compared to the fluorescence of the positive control with 99.7% positivity. However, cells treated with inhibitors from both the macropino/phagocytosis and clathrin-mediated pathways exhibited steeper drops in fluorescence, 16.8% and 20.8% loss of fluorescence respectively, compared to cells treated with inhibitors from the lipid raft/caveolae pathway, with only a 12.5% loss of fluorescence. This is demonstrated visually in Figure 7a and in a table in Figure 7c. Some cells treated with these inhibitors displayed nanoparticle on the surface but lacked nanoparticle in the cytoplasm, indicated by the arrows in Figure 7b, and suggesting those cells were unable to internalize the nanoparticle. This all seems to indicate that, not only do bisphosphonate-

conjugated silica nanoparticles utilize multiple pathways for internalization, but that the primary pathways of internalization are clathrin-mediated and macropino/phagocytosis in RAW 264.7 cells. Contrarily, the primary pathway utilized by OH-terminated silica nanoparticles in MC3T3-E1 cells is lipid raft/caveolae. In summary, both nanoparticles have slight differences in terms of the primary pathways used for internalization in osteoclast and osteoblast precursor cells, indicating that different cell types might utilize different pathways of internalization.

3.5 Colocalization assay of bisphosphonate-conjugated silica nanoparticles

Colocalization assays were conducted to elucidate the specific localization of bisphosphonate-conjugated silica nanoparticles following internalization within RAW 264.7 cells. Previous studies have demonstrated localization of OH-terminated silica nanoparticles to the endosome and lysosome in osteoblasts, but localization of bisphosphonate-conjugated silica nanoparticles has yet to be determined [11].

Endocytic colocalization was measured using FITC-conjugated transferrin. RAW 264.7 cells were incubated with internalization media and 10μg/ml NP-BisPO4 for 2 hours after which 25μg/ml FITC-transferrin was added for 30 minutes before imaging. Lysosomal trafficking was measured with LysoTracker Green. Cells were incubated with 10μg/ml NP-BisPO4 overnight, incubated in internalization media for 4 hours, and further incubated with 100nM LysoTracker Green for 30 minutes before imaging.

Endocytic trafficking images depicted significant overlap with a Pearson's correlation coefficient of 0.70 ± 0.09 between the endocytic markers and the bisphosphonate-conjugated silica nanoparticles as shown in the composite photo on Figure 8a, indicating localization of bisphosphonate-conjugated silica nanoparticles to the endosome. Lysosomal trafficking images also depicted significant overlap between the lysosomal markers and bisphosphonate-conjugated silica nanoparticles after 24 hours as shown in the composite photo on Figure 8b, indicating localization to the lysosome as well with a Pearson's correlation coefficient of 0.81 ± 0.08.

3.6 XTT assay of bisphosphonate-conjugated silica nanoparticles

XTT assays were conducted to determine the viability of RAW 264.7 cells treated with the bisphosphonate-conjugated silica nanoparticles. Silica nanoparticles are not toxic in the strictest sense, but when an excessive number of nanoparticles are internalized by a cell, the cell's ability to function properly is impeded, resulting in reduced cell viability [33].

Cell viability was measured using an XTT assay. RAW 264.7 cells were treated with either bisphosphonate-conjugated or OH-terminated silica nanoparticles at 100, 50, 25, 12.5, 6.25, 3.125, and 1.5 μg/ml concentrations or Alendronate at 100, 50, 25, 10, 5, 1, 0.5, and .1μM concentrations and then treated with XTT reagent. After 24 and 48 hours, the plates were read, and viability was determined compared to untreated controls. For both the 24 and 48 hour time points, similar trends are exhibited for each of the treatment groups. Alendronate showed no discernible change in viability at any of the concentrations tested. OH-terminated silica nanoparticles exhibited a significant increase in viability between 1.5 and 6μM with viability at 12μM being comparable to control. However, at higher concentrations there is a significant decrease in viability compared to control. Bisphosphonate-conjugated nanoparticles, contrarily, exhibited a steady and significant increase in viability over the baseline as concentration increased to approximately 200% viability at both 24 and 48 hours. However, this increase in

viability is primarily reflective of proliferation of cells over time. In summary, at both time points, alendronate resulted in no significant change in viability, bisphosphonate-conjugated silica nanoparticles resulted in an increase in viability, largely due to increasing cell number and OH-terminated silica nanoparticles demonstrated a steady decrease in viability at concentrations higher than 6μM.

A

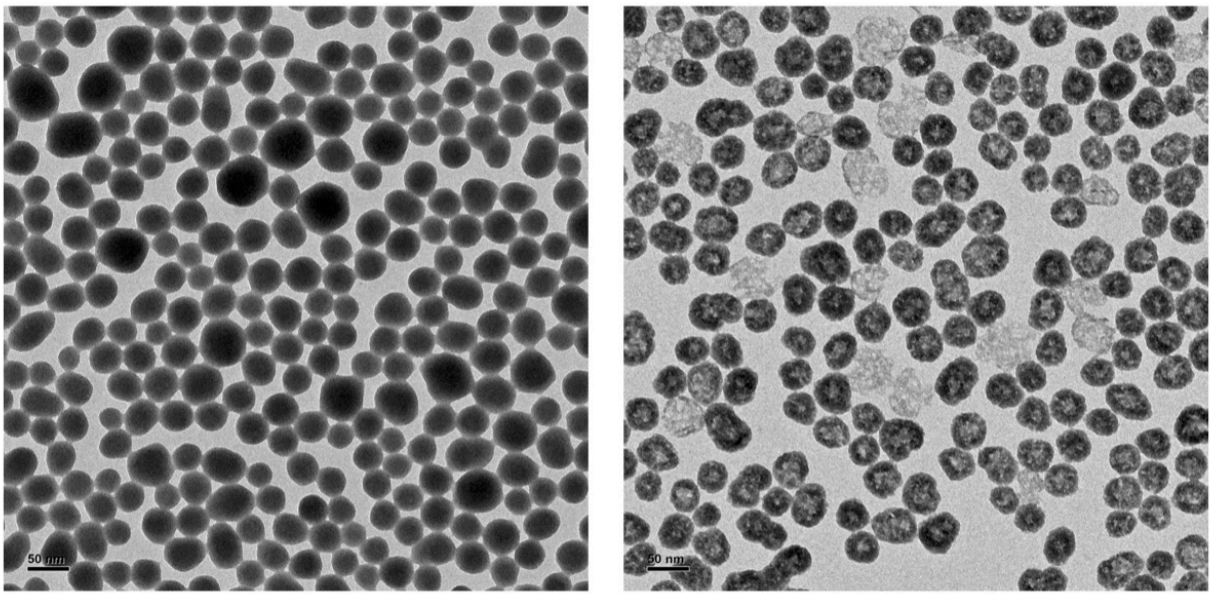

B

	NP-OH	NP-BisPO4
Size: Dynamic Light Scattering (Mean Number in nm)	42.4 ± 9.2	40.6 ± 7.8

Figure 1. Characterization of OH-terminated silica nanoparticles and bisphosphonate-conjugated silica nanoparticles. A) Transmission electron microscopy (TEM) images of OH-terminated nanoparticles (left) and bisphosphonate-conjugated nanoparticles (right). B) Dynamic light scattering (DLS) measurements for size on both nanoparticles.

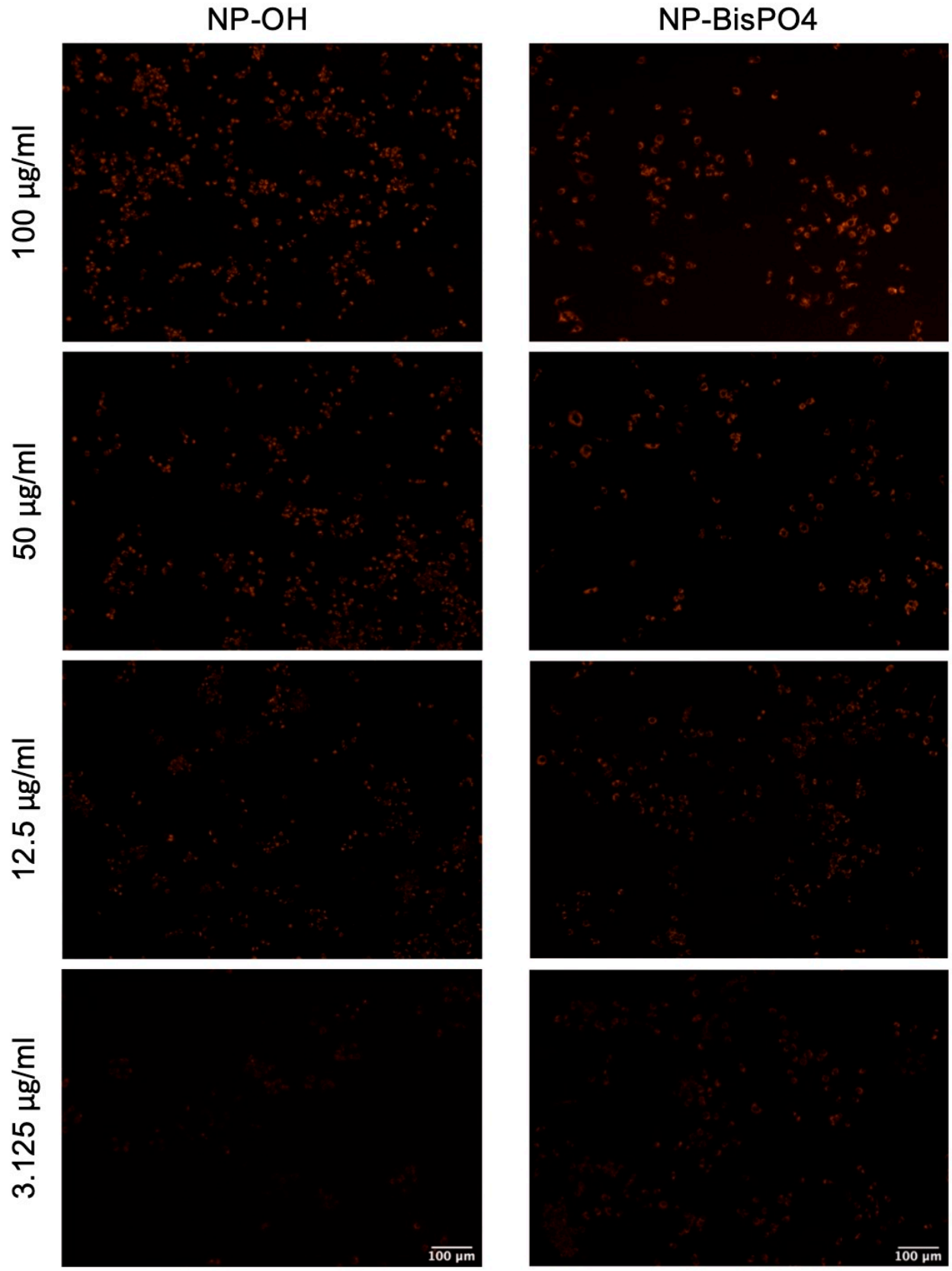

Figure 2. Dose-response internalization of OH-terminated and bisphosphonate-conjugated silica nanoparticles in RAW 264.7 cells. 50,000 cells were seeded in a 24-well plate and treated with various concentrations of either NP-OH or NP-BisPO4. After 24 hours, all the wells were fixed and representative images are displayed above, comparing NP-OH on the left and NP-BisPO4 on the right.

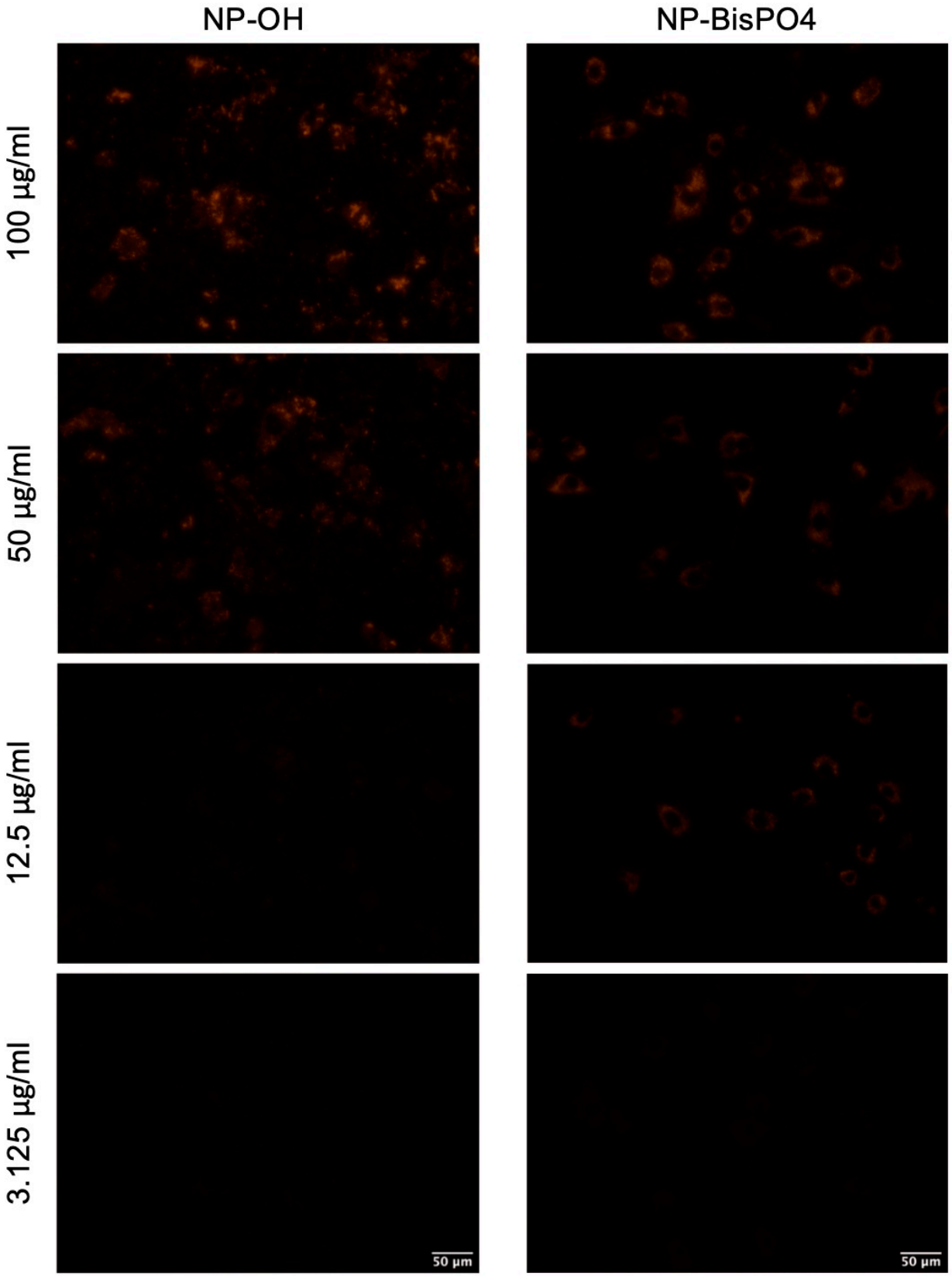

Figure 3. Dose-response internalization of OH-terminated and bisphosphonate-conjugated silica nanoparticles in MC3T3-E1 cells. 50,000 cells were seeded in a 24-well plate and treated with various concentrations of either NP-OH or NP-BisPO4. After 24 hours, all the wells were fixed and representative images are displayed above, comparing NP-OH on the left and NP-BisPO4 on the right.

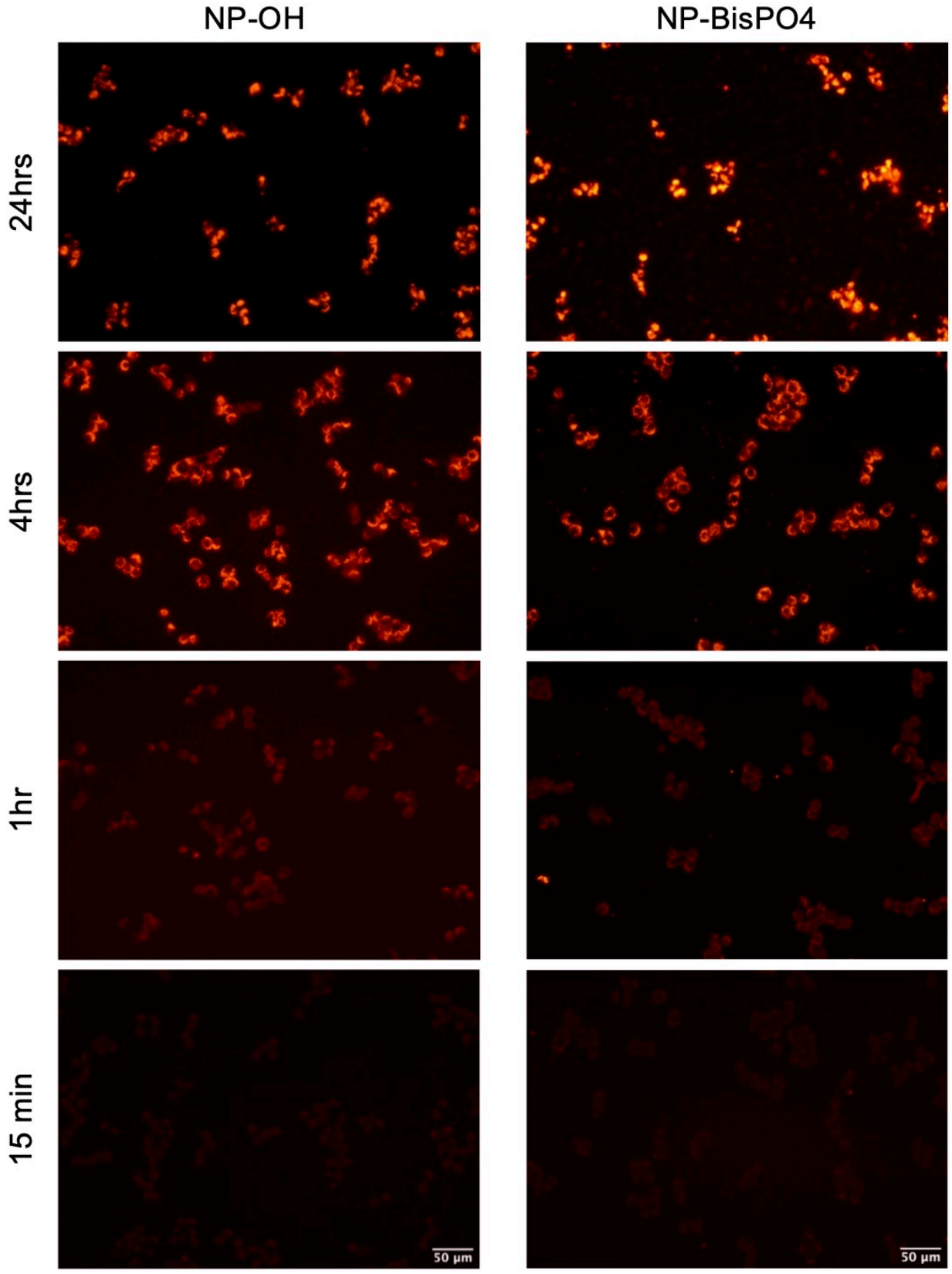

Figure 4. Time-course internalization of OH-terminated and bisphosphonate-conjugated silica nanoparticles in RAW 264.7 cells. 50,000 cells were seeded in a 24-well plate and treated with either 100µg /ml NP-OH or NP-BisPO4. Cells were fixed after various time points and representative images are displayed above, comparing NP-OH on the left and NP-BisPO4 on the right.

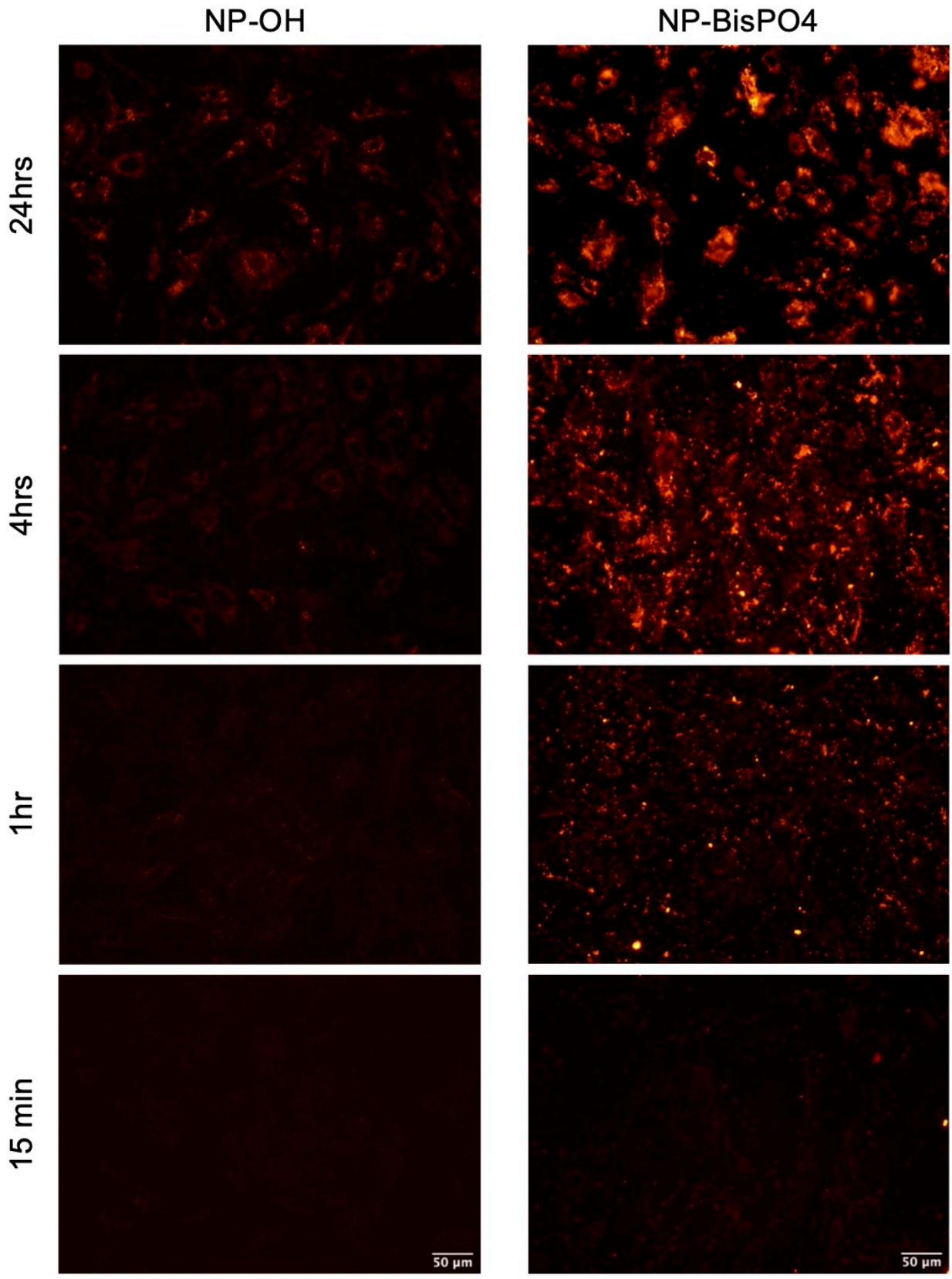

Figure 5. Time-course internalization of OH-terminated and bisphosphonate-conjugated silica nanoparticles in MC3T3-E1 cells. 50,000 cells were seeded in a 24-well plate and treated with either 100µg/ml NP-OH or NP-BisPO4. Cells were fixed after various time points and representative images are displayed above, comparing NP-OH on the left and NP-BisPO4 on the right.

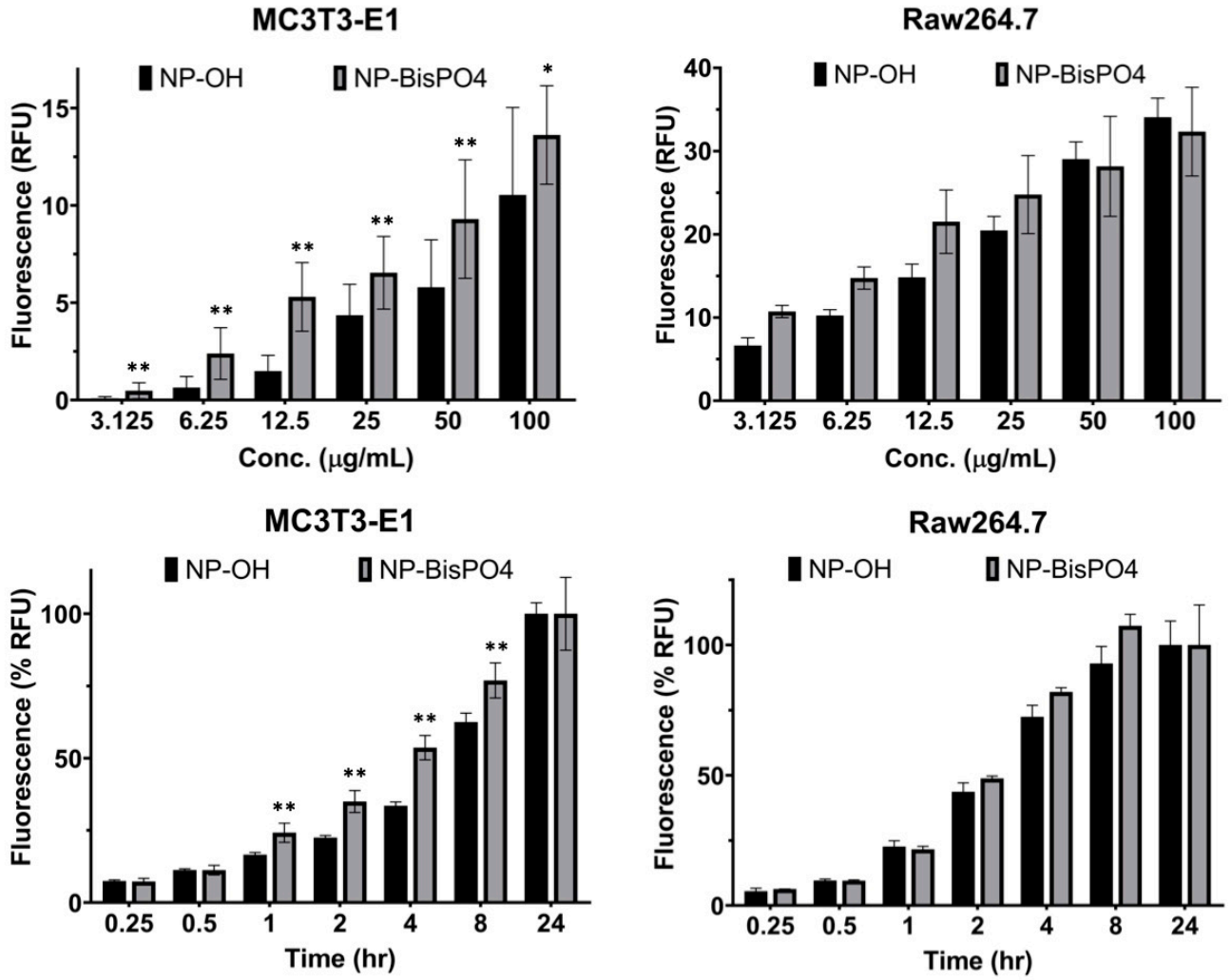

Figure 6. Dose-response and time-course assays in RAW 264.7 and MC3T3-E1 cells. Approx. 50 cells from each treatment group in RAW 264.7 cell studies and approx. 30 cells from each treatment group in MC3T3-E1 studies were measured for their mean gray value. Averages from each treatment group are displayed for both nanoparticles in the dose-response graphs. In the time-course graphs, values are displayed as a percentage of max fluorescence. **p <0.0001, **p <0.005

A

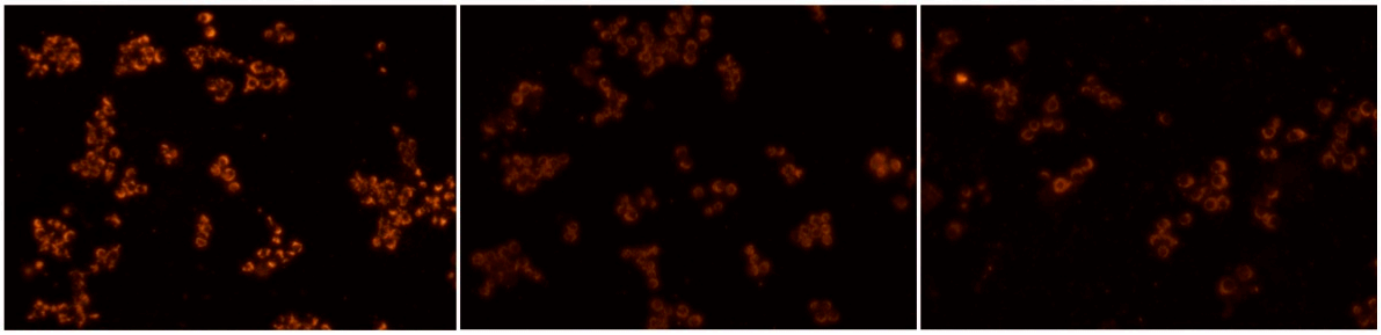

Macropino/Phagocytosis (Amiloride) | Clathrin-mediated (Chlorpromazine) | Lipid raft/caveolae (Nystatin)

B

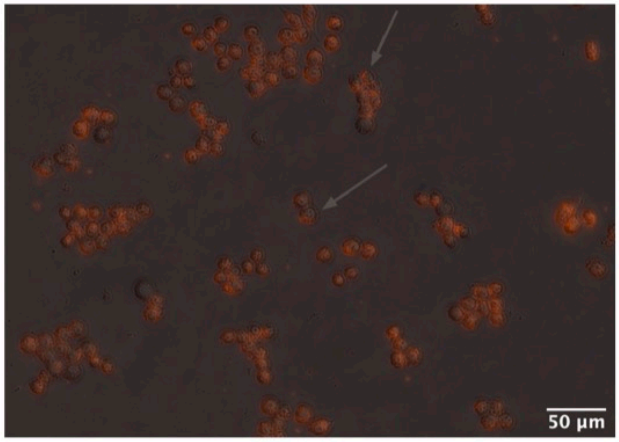

Chlorpromazine Overlay

C

Inhibitor	Target	Conc.	Total # of cells	# of fluorescent cells	% of fluorescent cells
Methyl ß-cyclodextrin (MßCD)	Lipid raft/Caveolae	7.5mM	58	51	87.9
Nystatin		50µM	317	276	87.1
Phenylarsine oxide	Clathrin-mediated	0.5µM	295	230	77.9
Chlorpromazine		25µM	522	420	80.5
Amiloride	Macropino/Phago-cytosis	1mM	675	566	83.9
Cytochalasin D		10µM	428	353	82.5

Figure 7. Endocytosis assays of bisphosphonate-conjugated silica nanoparticles in RAW 264.7 cells. A) Fluorescent images depicting one inhibitor from each of the three primary pathways of internalization. B) Overlaid fluorescence on brightfield images from the clathrin-mediated internalization pathways. Arrows pointing to cells with nanoparticle on the surface but not in the cytoplasm to demonstrate disruption of internalization. C) A table detailing the total and fluorescent cell counts from all images per treatment group.

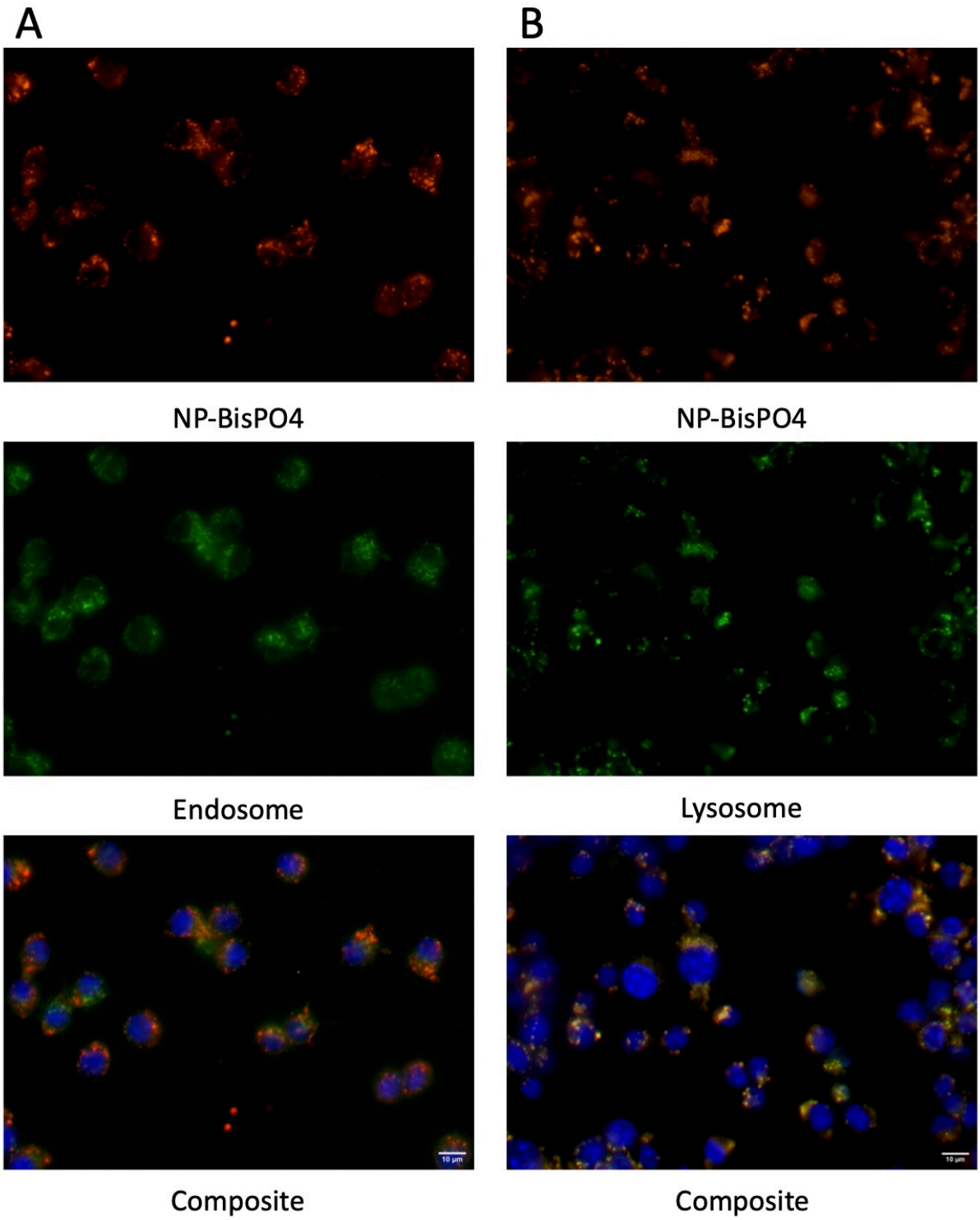

Figure 8. Localization assays of bisphosphonate-conjugated silica nanoparticles in RAW 264.7 cells. A) Endocytic trafficking was measured with FITC-conjugated transferrin. Cells were incubated with internalization media and 10µg/ml NP-BisPO4 for 2 hours following which 25µg/ml FITC-transferrin was for 30 minutes before imaging. B) Lysosomal trafficking was measured with LysoTracker Green. Cells were incubated with 10µg/ml NP-BisPO4 overnight, incubated in internalization media for 4 hours, and incubated with 100nM LysoTracker Green for a further 30 minutes before imaging.

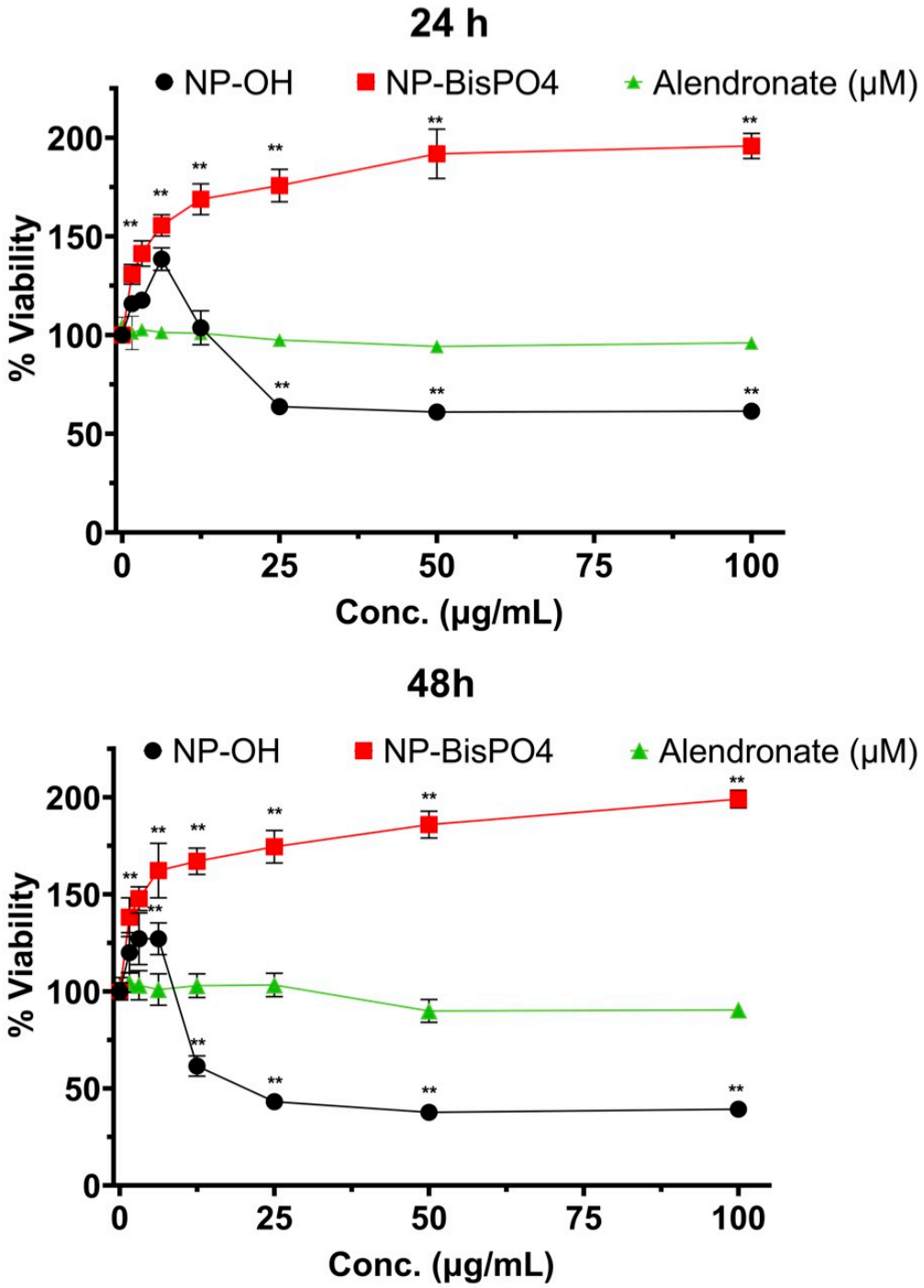

Figure 9. XTT viability assay of bisphosphonate-conjugated silica nanoparticles in RAW 264.7 cells. Cells were treated with either bisphosphonate-conjugated or OH-terminated silica nanoparticles at 100, 50, 25, 12.5, 6.25, 3.125, and 1.5 μg/ml concentrations or Alendronate at 100, 50, 25, 10, 5, 1, 0.5, and .1μM concentrations and then treated with XTT reagent. After 24 and 48 hours, viability was assessed. *p <0.005, **p <0.0001

4. Discussion

Both nanoparticles were characterized for their size and shape using TEM and DLS which determined that both particles have similar size and appearance, shared characteristics that will ideally translate to similar functional characteristics in cells.

Our dose-response assays have shown that OH-terminated silica nanoparticles and bisphosphonate-conjugated silica nanoparticles exhibit similar internalization in RAW 264.7 cells and slightly different ones in MC3T3-E1 cells. In MC3T3-E1 cell lines, bisphosphonate-conjugated silica nanoparticles are internalized at a significantly faster rate, but the gap becomes less significant at higher concentrations. Due to the fact that neither nanoparticle reached saturation within the bounds of the experiment, exhibited by the wide error margins of the EC_{50} data, further testing with higher concentrations will be needed to determine if this trend holds true. In the RAW 264.7 cells, EC_{50} analysis lends itself to the idea that bisphosphonate-conjugated silica nanoparticles are internalized at a faster rate but there exists no significant gap between the two nanoparticle internalizations. Finally, the overall fluorescence levels in the MC3T3-E1 cells are consistently lower than the fluorescence levels in the RAW 264.7 cells. This difference might be due to the large size of MC3T3-E1 cells as compared to RAW 264.7 cells or just a lower rate of internalization of nanoparticles into MC3T3-E1 cells.

In the time-course assays, the differences between each nanoparticle at different time points stay fairly consistent for both cell lines. As the fluorescence levels in RAW 264.7 cells are consistently higher as compared to uptake in the MC3T3-E1 cells at the same time points, the graphs were formatted to display fluorescence as a percentage of total saturation. Although there is no significant difference between the two nanoparticles at any time point for the RAW 264.7 cells, bisphosphonate-conjugated nanoparticles exhibit a significantly higher fluorescence at 1, 2, 4 and 8 hour time points as compared to OH-terminated silica nanoparticles in MC3T3-E1 cells. This indicates that bisphosphonate-conjugated silica nanoparticles are internalized at a slightly greater rate, a trend consistent with the dose-dependent data. Additionally, the time-dependent graphs indicate that both nanoparticles reach saturation in the RAW 264.7 cells around 8 hours and saturation is never reached in in the MC3T3-E1 cells, another indication that experiments with higher concentrations are needed in MC3T3-E1 cells. This is further consistent with the dose-response data which showed lower levels of fluorescence in MC3T3-E1 cells as compared to RAW 264.7 at the same concentration and indicates that MC3T3-E1 cells may have a slower rate of internalization of both nanoparticles.

Previous studies have shown that OH-terminated silica nanoparticles predominantly utilize the lipid raft/caveolae internalization pathways in MC3T3-E1 cells [11]. Through our endocytosis assay, we determined that the bisphosphonate-conjugated silica nanoparticles likely utilized all three endocytosis pathways to varying degrees in RAW 264.7 cells, although the clathrin-mediated and macropino/phagocytosis pathways are the primary methods of internalization.

Specifically for cells treated with inhibitors for the clathrin-mediated and macropino/phagocytosis pathways, many of the cells exhibited a common trait. Nanoparticles appears in a thin stretch on the surface of the cell but not in the cytoplasm which indicates the ability of the nanoparticle to target the cell, but an inability of the cell to internalize the nanoparticle. Cells exhibiting this phenomenon are designated in Figure 7b and indicated by gray arrows.

This appearance was not present in cells treated with inhibitors for the lipid raft/caveolae but there was still a marked decrease in the number of fluorescent cells. Therefore, it is likely that bisphosphonate-bound silica nanoparticles utilize all three pathways, if to varying degrees. Additionally, it makes sense that bisphosphonate-conjugated display this phenomenon as alendronate is thought to improve targeting in addition to intestine absorption. Subsequently, bisphosphonate-conjugated silica nanoparticle is likely targeted to the RAW 264.7 cells, sticking to the surface, and unable to be internalized in the presence of inhibitors.

In summary, the endocytosis assay data indicates that the different cell types use slightly different pathways to internalize nanoparticles. The RAW 264.7 cells use of all three pathways for internalization of the bisphosphonate-conjugated silica nanoparticle is likely due to its descent from a macrophage lineage and the necessity for cells in this line to internalize to a great degree. This is also consistent with other studies examining nanoparticle internalization in RAW 264.7 cells in which all three pathways for internalization are utilized [35]. Additionally, this would account for the vast differences between internalization between RAW 264.7 cells and MC3T3-E1 cells, as RAW 264.7 cells consistently exhibited higher levels of fluorescence, and therefore higher levels of internalization, at every time and dose point as compared to MC3T3-E1 cells.

In the colocalization studies, it was established that bisphosphonate-conjugated silica nanoparticles colocalize with endocytic markers and with lysosomal markers at later time points, indicating localization within RAW 264.7 cells to the endosome and the lysosome. This data is consistent with previous studies in which OH-terminated silica nanoparticles also localized to the endosome and lysosome in MC3T3-E1 cells [11]. However, it is interesting to note that localization with endosomal markers appears as early as 2 hours but significant overlap with lysosomal markers does not occur until 24 hours. This indicates that when bisphosphonate-conjugated silica nanoparticles are internalized, they localize first to the endosome and then travel to the lysosome, a pattern consistent with OH-terminated silica nanoparticles in MC3T3-E1 cells [11]. This assessment of localization is one of the first steps in determining the mechanisms of action of bisphosphonate-conjugated silica nanoparticles and the similarly between the nanoparticles so far is an encouraging sign. Ideally, this shared localization pattern will lend itself to shared effects in bone cells.

Finally, XTT assays were performed to assess the viability of cells treated with both nanoparticles. This assay was conducted in RAW 264.7 cells at both 24 and 48 hour time points but both graphs conclusively show stable trends for all three treatment groups. Alendronate has no discernible effect on viability which is to be expected from past studies regarding the effects of alendronate on bone cells [24]. OH-conjugated silica nanoparticle treatment is correlated with a steady decrease of cell viability as the concentration increases above 6μg/ml. As previously stated, silica nanoparticles do not display toxicity in a traditional way, but an excess of nanoparticles within a cell can lead to loss of function [33]. Bisphosphonate-conjugated silica nanoparticles, however, are associated with a steady increase in viability at all concentrations tested. This increased viability over control is indicative of an increase in cell number due to increased proliferation. If bisphosphonate-conjugated silica nanoparticles have the ability to prevent differentiation without impeding the function of the cells, proliferation could continue and produce the viability trends displayed in Figure 9 [34].

Moving forward, more assays are needed to establish the mechanistic action of bisphosphonate-conjugated nanoparticles within osteoclasts and osteoblasts. Previous studies have shown that OH-terminated silica nanoparticles have the ability to inhibit osteoblast activity

and promote osteoclast activity *in vitro* and *in vivo* [10]. Tartrate-resistant acid phosphatase (TRAP) is used to check for differentiated osteoclasts and when treated with bisphosphonate-conjugated silica nanoparticles, should display lower levels of mature osteoclasts [18]. Several attempts to perform TRAP assays have proved unsuccessful, likely due to the cell culture pH not being conducive to a productive stain [19]. However, in the few plates which have stained, bisphosphonate-conjugated silica nanoparticle treated wells appear to contain fewer differentiated osteoclasts but more non-differentiated osteoclasts than seen with OH-terminated suggesting that the bisphosphonate-conjugated silica nanoparticles are not causing significant cell death. Further TRAP staining will be required to confirm these preliminary findings. Similarly, alkaline phosphatase (ALP) staining is used to check for differentiated osteoblasts [20]. These assays have been largely ineffectual as well due to weak staining caused by low cell seeding density. While further testing is required, certain stains seem to show a promotion of osteoblast differentiation.

Additionally, PCR should be performed in both RAW 264.7 and MC3T3-E1 cells treated with both nanoparticles to assess for genes involved in bone cell differentiation and autophagy, such as TRAP, OC-STAMP, LC3, and Nfatc-1, as OH-terminated silica nanoparticles have been shown to act in the autophagy pathway [11, 21]. Following these functional assays, the next step is to move into mice experiments. OH-terminated silica nanoparticles have been shown to restore bone density *in vivo*, however, it is believed that absorption in the intestines would be minimal if given orally [12, 23]. In order to improve oral absorption and targeting a bisphosphonate, alendronate, was added to the surface of the silica nanoparticle [24]. It's been established in this study that OH-terminated silica nanoparticles and bisphosphonate-conjugated nanoparticles exhibit very similar internalization patterns in pre-osteoblasts and pre-osteoclasts cell lines *in vitro*. Assays should also be performed to determine the internalization patterns of both OH-terminated and bisphosphonate-conjugated in intestinal cells such as Caco2 cells [23]. If bisphosphonate-conjugated nanoparticles do demonstrate improved targeting and absorption, this means that a smaller concentration of bisphosphonate-conjugated silica nanoparticles can exhibit the same effect as a larger concentration of OH-terminated silica nanoparticles when given experimentally as treatment. Therefore, bisphosphonate-conjugated silica nanoparticles would work as an effective, orally administered treatment for osteoporosis.

5. Conclusion

In conclusion, our dose-response and time-course assays show that, excluding minor differences at low concentrations and short time points, both the OH-terminated silica nanoparticle and bisphosphonate-conjugated silica nanoparticle exhibit similar internalization patterns in RAW 264.7 cells and MC3T3-E1 cells. Further, the endocytosis assays indicate that RAW 264.7 cells and MC3T3-E1 cells utilize slightly different pathways for internalization, with lipid raft/caveolae being the primary pathway in MC3T3-E1 cells and all three pathways being utilized to some extent in the RAW 264.7 cells. This use of multiple pathways might also help explain the greater speed with which the osteoclast precursor cells internalize nanoparticle as opposed to the osteoblast precursor cells. However, once inside the cells, both nanoparticles exhibit the same internalization pattern – localizing first to the endosome and later to the lysosome, indicated potential for shared mechanisms of action within bone cells.

Further studies will examine the effects of bisphosphonate-conjugated silica nanoparticles on osteoblast and osteoclast differentiation and determine the role it plays in the

autophagy pathway. Eventually, studies *in vivo* will be able to determine the overall efficacy of bisphosphonate-conjugated silica nanoparticles as an effective osteoporosis treatment. However, for now, this study is the first step in further understanding bisphosphonate-conjugated silica nanoparticles at the cellular level.

6. References

1. Salata, O. Applications of nanoparticles in biology and medicine. *J Nanobiotechnol* **2,** 3 (2004). https://doi.org/10.1186/1477-3155-2-3
2. Murthy SK. Nanoparticles in modern medicine: state of the art and future challenges. *Int J Nanomedicine*. 2007;2(2):129-141.
3. Rahman, I. A., & Padavettan, V. (2012). Synthesis of Silica nanoparticles by Sol-Gel: Size-dependent properties, surface modification, and applications in silica-polymer nanocompositesa review. *Journal of Nanomaterials*. https://doi.org/10.1155/2012/132424
4. S.W. Ha, M.N. Weitzmann, G.R. Beck Jr, Dental and Skeletal Applications of Silica-Based Nanomaterials, in: K. Subramani, W. Ahmed, J. Hartsfield (Eds.), Nanobiomaterials in Clinical Dentistry, William Andrew Publishing, Oxford, UK, 2013, pp. 69–91.
5. A. Albanese, P.S. Tang, W.C. Chan, The effect of nanoparticle size, shape, and surface chemistry on biological systems, Annu. Rev. Biomed. Eng. (2012).
6. B. Clarke, Normal bone anatomy and physiology, Clin. J. Am. Soc. Nephrol. 3 (Suppl 3) (2008) S131–S139.
7. Office of the Surgeon General (US). Bone Health and Osteoporosis: A Report of the Surgeon General. Rockville (MD): Office of the Surgeon General (US); 2004. 2, The Basics of Bone in Health and Disease. Available from: https://www.ncbi.nlm.nih.gov/books/NBK45504/
8. Föger-Samwald U, Dovjak P, Azizi-Semrad U, Kerschan-Schindl K, Pietschmann P. Osteoporosis: Pathophysiology and therapeutic options. *EXCLI J*. 2020;19:1017-1037. Published 2020 Jul 20. doi:10.17179/excli2020-2591
9. Tu KN, Lie JD, Wan CKV, et al. Osteoporosis: A Review of Treatment Options. *P T*. 2018;43(2):92-104.
10. G.R. Beck Jr., S.W. Ha, C.E. Camalier, M. Yamaguchi, Y. Li, J.K. Lee, M.N. Weitzmann, Bioactive silica-based nanoparticles stimulate bone-forming osteoblasts, suppress bone-resorbing osteoclasts, and enhance bone mineral density in vivo, Nanomedicine 8 (2012) 793–803.
11. S.W. Ha, M.N. Weitzmann, G.R. Beck Jr., Bioactive silica nanoparticles promote osteoblast differentiation through stimulation of autophagy and direct association with LC3 and p62, ACS Nano 8 (2014) 5898–5910.
12. M.N. Weitzmann, S.W. Ha, T. Vikulina, S. Roser-Page, J.K. Lee, G.R. Beck Jr., Bioactive silica nanoparticles reverse age-associated bone loss in mice, Nanomedicine 11 (2015) 959–967.
13. Drake MT, Clarke BL, Khosla S. Bisphosphonates: mechanism of action and role in clinical practice. *Mayo Clin Proc*. 2008;83(9):1032-1045. doi:10.4065/83.9.1032
14. Vincent C, Kogawa M, Findlay DM, Atkins GJ. The generation of osteoclasts from RAW 264.7 precursors in defined, serum-free conditions. *J Bone Miner Metab*. 2009;27(1):114-119. doi:10.1007/s00774-008-0018-6

15. Ha SW, Viggeswarapu M, Habib MM, Beck GR Jr. Bioactive effects of silica nanoparticles on bone cells are size, surface, and composition dependent. *Acta Biomater*. 2018;82:184-196. doi:10.1016/j.actbio.2018.10.018
16. Gisbert-Garzarán M, Manzano M, Vallet-Regí M. Mesoporous Silica Nanoparticles for the Treatment of Complex Bone Diseases: Bone Cancer, Bone Infection and Osteoporosis. *Pharmaceutics*. 2020;12(1):83. Published 2020 Jan 20. doi:10.3390/pharmaceutics12010083
17. Kumari, S., MG, S. & Mayor, S. Endocytosis unplugged: multiple ways to enter the cell. *Cell Res* **20,** 256–275 (2010). https://doi.org/10.1038/cr.2010.19
18. Lindunger A, MacKay CA, Ek-Rylander B, Andersson G, Marks SC Jr. Histochemistry and biochemistry of tartrate-resistant acid phosphatase (TRAP) and tartrate-resistant acid adenosine triphosphatase (TrATPase) in bone, bone marrow and spleen: implications for osteoclast ontogeny. *Bone Miner*. 1990;10(2):109-119. doi:10.1016/0169-6009(90)90086-u
19. Halling Linder C, Ek-Rylander B, Krumpel M, et al. Bone Alkaline Phosphatase and Tartrate-Resistant Acid Phosphatase: Potential Co-regulators of Bone Mineralization. *Calcif Tissue Int*. 2017;101(1):92-101. doi:10.1007/s00223-017-0259-2
20. Liu, B., Lu, Y., Wang, Y. *et al.* A protocol for isolation and identification and comparative characterization of primary osteoblasts from mouse and rat calvaria. *Cell Tissue Bank* **20,** 173–182 (2019). https://doi.org/10.1007/s10561-019-09751-0
21. Montaseri A, Giampietri C, Rossi M, Riccioli A, Del Fattore A, Filippini A. The Role of Autophagy in Osteoclast Differentiation and Bone Resorption Function. *Biomolecules*. 2020;10(10):1398. Published 2020 Sep 30. doi:10.3390/biom10101398
22. Bharti C, Nagaich U, Pal AK, Gulati N. Mesoporous silica nanoparticles in target drug delivery system: A review. *Int J Pharm Investig*. 2015;5(3):124-133. doi:10.4103/2230-973X.160844
23. Ye D, Bramini M, Hristov DR, et al. Low uptake of silica nanoparticles in Caco-2 intestinal epithelial barriers. *Beilstein J Nanotechnol*. 2017;8:1396-1406. Published 2017 Jul 7. doi:10.3762/bjnano.8.141
24. Porras AG, Holland SD, Gertz BJ. Pharmacokinetics of alendronate. *Clin Pharmacokinet*. 1999;36(5):315-328. doi:10.2165/00003088-199936050-00002
25. Leu, C. T., Luegmayr, E., Freedman, L. P., Rodan, G. A., & Reszka, A. A. (2006). Relative binding affinities of bisphosphonates for human bone and relationship to antiresorptive efficacy. *Bone*, *38*(5), 628–636. https://doi.org/10.1016/j.bone.2005.07.023
26. Bliuc, D., Nguyen, N. D., Milch, V. E., Nguyen, T. V., Eisman, J. A., & Center, J. R. (2009). Mortality risk associated with low-trauma osteoporotic fracture and subsequent fracture in men and women. *JAMA*, *301*(5), 513–521. https://doi.org/10.1001/jama.2009.50
27. Lee, J. A., Kim, M. K., Paek, H. J., Kim, Y. R., Kim, M. K., Lee, J. K., Jeong, J., & Choi, S. J. (2014). Tissue distribution and excretion kinetics of orally administered silica nanoparticles in rats. *International journal of nanomedicine*, *9 Suppl 2*(Suppl 2), 251–260. https://doi.org/10.2147/IJN.S57939
28. Farrell, K. B., Karpeisky, A., Thamm, D. H., & Zinnen, S. (2018). Bisphosphonate conjugation for bone specific drug targeting. *Bone reports*, *9*, 47–60. https://doi.org/10.1016/j.bonr.2018.06.007

29. Lee, D., Heo, D., Kim, HJ. *et al.* Inhibition of Osteoclast Differentiation and Bone Resorption by Bisphosphonate-conjugated Gold Nanoparticles. *Sci Rep* **6,** 27336 (2016). https://doi.org/10.1038/srep27336
30. Quarles LD, Yohay DA, Lever LW, Caton R, Wenstrup RJ. Distinct proliferative and differentiated stages of murine MC3T3-E1 cells in culture: an in vitro model of osteoblast development. *J Bone Miner Res*. 1992;7(6):683-692. doi:10.1002/jbmr.5650070613
31. Schindelin J, Arganda-Carreras I, Frise E, et al. Fiji: an open-source platform for biological-image analysis. *Nat Methods*. 2012;9(7):676-682. Published 2012 Jun 28. doi:10.1038/nmeth.2019
32. Zhao H. Membrane trafficking in osteoblasts and osteoclasts: new avenues for understanding and treating skeletal diseases. *Traffic*. 2012;13(10):1307-1314. doi:10.1111/j.1600-0854.2012.01395.x
33. Kim IY, Joachim E, Choi H, Kim K. Toxicity of silica nanoparticles depends on size, dose, and cell type. *Nanomedicine*. 2015;11(6):1407-1416. doi:10.1016/j.nano.2015.03.004
34. Cooper GM. The Cell: A Molecular Approach. 2nd edition. Sunderland (MA): Sinauer Associates; 2000. Cell Proliferation in Development and Differentiation. Available from: https://www.ncbi.nlm.nih.gov/books/NBK9906/
35. Plummer EM, Manchester M. Endocytic uptake pathways utilized by CPMV nanoparticles. *Mol Pharm*. 2013;10(1):26-32. doi:10.1021/mp300238w